

# Unreading Race: Purging Protected Features from Chest X-ray Embeddings

Tobias Weber<sup>1,2,3</sup>, Michael Ingrischi<sup>2,3</sup>, Bernd Bischl<sup>1,3</sup>, and David Rügamer<sup>1,3</sup>

<sup>1</sup>Department of Statistics, LMU Munich

<sup>2</sup>Department of Radiology, University Hospital, LMU Munich

<sup>3</sup>Munich Center for Machine Learning (MCML)

tobias.weber@stat.uni-muenchen.de

## Abstract

**Purpose** To analyze and remove protected feature effects in chest radiograph embeddings of deep learning models.

**Materials and Methods** An orthogonalization is utilized to remove the influence of protected features (e.g., age, sex, race) in chest radiograph embeddings, ensuring feature-independent results. To validate the efficacy of the approach, we retrospectively study the MIMIC and CheXpert datasets using three pre-trained models, namely a supervised contrastive, a self-supervised contrastive, and a baseline classifier model. Our statistical analysis involves comparing the original versus the orthogonalized embeddings by estimating protected feature influences and evaluating the ability to predict race, age, or sex using the two types of embeddings.

**Results** Our experiments reveal a significant influence of protected features on predictions of pathologies. Applying orthogonalization removes these feature effects. Apart from removing any influence on pathology classification, while maintaining competitive predictive performance, orthogonalized embeddings further make it infeasible to directly predict protected attributes and mitigate subgroup disparities.

**Conclusion** The presented work demonstrates the successful application and evaluation of the orthogonalization technique in the domain of chest X-ray classification.

# 1 Introduction

At the interdisciplinary intersection between computer science and radiological imaging, the applications of deep learning for the analysis of chest X-ray (CXR) images have garnered considerable attention. Besides the fact that CXR imaging remains a cornerstone of diagnostic imaging, this can largely be attributed to the availability of extensive, annotated datasets, e.g., [1, 2, 3], which allows the utilization of deep learning algorithms for a variety of research questions. Among others, these tasks include classification [2], image generation [3, 4], image manipulation [5], report generation [6], and self-supervised pre-training [7, 8]. With growing public interest and application in practice, there is an escalating demand for fairness, transparency, and explicability of such machine learning models. This need is paramount in the context of clinical decision-making, where the primary concern is the patient’s outcome.

Of particular concern is the potential for bias in predictive models, which might lead to serious consequences in downstream applications. The work of Gichoya et al. [9] shows that deep learning models can predict a patient’s race in CXRs with high certainty, even when clinical experts cannot. Building on this observation, the recent study by [10] demonstrates that features like age, sex, and race are already encoded in deep feature representations of neural CXR classifiers and thus can have a strong influence on downstream prediction tasks. Even more concerning, this property is not restricted to classifiers but also extends to embeddings obtained by contrastive methods, e.g., Google’s *Chest X-ray Foundation Model* [7, 11].

In the following, we define the term *protected features* as intrinsic characteristics typically protected by law against discrimination and bias. Not correcting for influences of protected features in predictions and representations used for decision-making can have detrimental effects. This could lead to CXR classifiers not fully generalizing to certain subgroups as found in [12] or to exhibit fairness concerns [13]. As noted by [10], ensuring fairness and equal treatment across all subgroups is a major challenge as training datasets tend to be imbalanced for specific populations.

The purpose of this work is twofold: First, we evaluate whether protected features significantly contribute to model predictions in classifiers based on CXR embeddings using three publicly available models and two open datasets. Second, we investigate whether the influence of the protected features can be removed by means of a recently proposed orthogonalization procedure [14, 15], resulting in unbiased deep representations of CXR images.

## 2 Materials and Methods

### 2.1 Orthogonalization

Whereas the following introduces the orthogonalization more formally, a geometric depiction of the approach is visualized in Figure 1. Let  $\mathbf{E} \in \mathbb{R}^{n \times d}$  be the embedding matrix of dimension  $d$  for  $n$  samples, and  $\mathbf{X} \in \mathbb{R}^{n \times p}$  a design matrix containing the information of  $p$  protected features for each sample. The ultimate goal is to eliminate feature effects of  $\mathbf{X}$  in  $\mathbf{E}$ . This can be achieved by projecting  $\mathbf{E}$  onto the space orthogonal to the space spanned by the columns of  $\mathbf{X}$ . For this, we construct  $\mathbf{Q} \in \mathbb{R}^{n \times q}$  using the QR-decomposition  $\mathbf{X} = \mathbf{Q}\mathbf{R} \in \mathbb{R}^{n \times p}$ . The projection matrix  $\mathcal{P}_{\mathbf{X}}$ , which projects an object, e.g.  $\mathbf{E}$ , onto the space spanned by the columns of  $\mathbf{X}$ , is then given by  $\mathbf{Q}\mathbf{Q}^\top$ , and its orthogonal complement  $\mathcal{P}_{\mathbf{X}}^\perp = \mathbf{I} - \mathcal{P}_{\mathbf{X}}$  with  $n$ -dimensional identity matrix  $\mathbf{I}$  [16]. Using this orthogonal projection matrix, we can obtain the corrected embedding

$$\tilde{\mathbf{E}} = \mathcal{P}_{\mathbf{X}}^\perp \mathbf{E} = (\mathbf{I} - \mathbf{Q}\mathbf{Q}^\top) \mathbf{E}. \quad (1)$$

The Frisch-Waugh-Lovell theorem [17] then guarantees that all  $\mathbf{X}$ -influence is subtracted from  $\tilde{\mathbf{E}}$ . In particular, this will result in a zero influence of any of the features in  $\mathbf{X}$  on  $\mathbf{E}$  when checking with a significance-test or linear model.

In order to apply this procedure for new unseen data  $\mathbf{E}^*$ , we derive  $\mathcal{P}_{\mathbf{X}^*} = \mathbf{Q}^* \mathbf{Q}^{*\top}$  from the associated protected features  $\mathbf{X}^*$  and subsequently compute the orthogonalized embedding  $\tilde{\mathbf{E}}^* = (\mathbf{I} - \mathcal{P}_{\mathbf{X}^*}) \mathbf{E}^*$ .

## 2.2 Datasets

The methodology is retrospectively evaluated on the MIMIC [1] and CheXpert [2] datasets (cf. Table 1), which both contain patients from US hospitals. The racial groups are derived in the same fashion as in [9, 11]. We apply the *U-zeros* strategy from [18] to define binary pathology labels.

**MIMIC** We utilize the recommended official training (42,148 patients with 181,342 scans) and test splits (257 patients with 3,041 scans) [1], which are contained in the published embeddings of the CXR foundation model [7]. The dataset shows a substantial racial imbalance, with 75.77% / 79.77% of patients being White, while Black and Asian patients constitute only 19.93% / 17.51 % and 4.30 % / 2.71 % in the train and test, respectively. A similar racial disparity is evident in the scan distribution. The age statistics reveal variations among racial and gender subgroups. In the training set, Black patients have a notably lower average age compared to White patients (62.6 versus 57.7 mean age).

**CheXpert** Our CheXpert subset consists of the same train (25,730 patients with 76,205 scans) and test (12,866 patients with 38,240 scans) split previously employed by [9] and [11] in their analyses. There is a notable disparity in patient demographics across racial and gender categories. White patients constitute the majority with 77.86% / 77.38 %, followed by Asians (15.33% / 15.79%), while Black patients are underrepresented (6.81% / 6.83%). Generally, Black patients in both the training and test sets tend to be younger on average (63.1 / 63.3 versus 55.7 / 57.4 mean age).

## 2.3 Analyzed Models

Our analysis includes the embeddings and feature representations of three models, each comprising different architectures and training procedures. We focus on publicly available and pretrained architectures and embeddings.

**CXR Foundation Model (CFM; [7])** This EfficientNet-L2 model [19] is trained on over 800,000 CXR images from India and the US using a supervised contrastive procedure [20] by differentiating between normal and abnormal samples. The model is only available using a restricted application-based API interface that offers 1376-dimensional feature embeddings. Thus, we utilize the publicly available and packaged embeddings of the MIMIC dataset.<sup>1</sup>

**CheSS [8]** With a ResNet-50 [21] as a basis, CheSS is a contrastive self-supervised model trained with the MoCo v2 strategy [22] on 4.8 million CXRs from South Korea. The model yields 2048-dimensional feature vectors.

**CheXNet Classifier (CLF, [18])** The CLF label represents a Densenet-121 classifier trained on MIMIC and CheXpert, respectively. The models are publicly available and obtained from the *torchxrayvision* library [23] yielding 1024-dimensional last-layer feature vectors.

## 2.4 Statistical Analysis

Our analysis consists of three parts, each evaluated on the original and orthogonalized embedding: Influence of protected features on pathology classification, direct prediction of protected information, and downstream task performance.

**Evaluating the Influence of Protected Features** We employ a linear evaluation protocol, using the embedding as the only feature to predict the different pathologies. Our prediction model of choice is a logistic regression, optimized in a gradient-based iterative fashion due to its capability of handling high-dimensionality in the feature embeddings. The implementation is done in PyTorch v2.0 [24]. The network is trained for 10 epochs with a learning rate of 0.0001 and batch size of 256. All metrics are evaluated over 10 random initializations. We do not conduct a hyperparameter

---

<sup>1</sup><https://doi.org/10.13026/pxc2-vx69>

search as the goal of this paper is not to beat the current state-of-the-art but to analyze and examine the effects of protected features on predictive performance.

In order to check the influence of protected features in the prediction model, we use a second linear model (the *evaluation model*) that estimates the influence of protected features on the predicted logits from the *prediction model*. From the evaluation model, we obtain regression coefficients for age, race, and sex to quantify their influence and also to assess their significance via the provided t-statistics and -tests.

**Extracting Protected Features** While the previous evaluation checks the influence of protected features on the model’s prediction when the goal is to classify pathologies, we additionally employ three (generalized) linear models to directly predict the protected information using the embedding. A linear model is used for the prediction of age, a logistic regression for the prediction of sex, and a multinomial regression to predict the three different race outcomes. All models are again trained using a gradient-based iterative procedure in PyTorch v2.0.

**Downstream Prediction Performance** Applying the orthogonalization method results in the transformation of the embedding vector. We investigate how the subsequent downstream pathology prediction performance is impacted, when removing protected feature information, using the previously trained CXR classifier models.

### 3 Results

#### 3.1 Influence of Protected Features on Predictions

The estimated influence of protected features for the labels *Pleural Effusion*, *Cardiomegaly*, and *No Finding* is given in Table 2. Extended results including the distribution of coefficients and p-values over multiple runs are found in Supplement A. The three labels are chosen due to their prevalence in the datasets.

**Without Orthogonalization** The majority of coefficients exhibit extremely small p-values, signaling a significant influence on the predictions. This highlights the substantial influence that protected features have on the model outputs. For example, in the case of the MIMIC CFM embeddings and *Pleural Effusion*, an increase of patient age of ten years results in a significant increase of  $0.1 \cdot 4.246 = 0.42$  in the predicted logits, or equivalent, a multiplicative increase in log-odds of almost 52% for the prediction model.<sup>2</sup>

Moreover, race also shows a significant influence, in particular being a Black instead of White patient, resulting in a reduction of the predicted probability for *Pleural Effusion*. The respective estimated additive effect  $-0.694$  results in logit values that imply a reduction of 50% in the log-odds for the prediction model. While being Black in the MIMIC CFM embedding is associated with a risk-reducing factor for *Pleural Effusion*, it increases for *Cardiomegaly* with a coefficient of 0.145.

Being female is generally associated with a negative coefficient with the exception of *Pleural Effusion* in the CheXpert CheSS embeddings (0.135). The coefficients for Asians exhibit relatively small values and, in many cases, p-values greater than 0.05, indicating a lack of statistical significance.

An interesting case is the label *No Finding*, which indicates the presence of a patient with no abnormalities. The obtained coefficients confirm our methodology, as their magnitudes are similar to *Pleural Effusion* and *Cardiomegaly* but are equipped with a flipped sign.

Overall, the analysis of MIMIC results in generally higher coefficients than CheXpert. When evaluating the CheSS embedding, e.g., the age coefficient for *Pleural Effusion* is 3.529 versus 1.679. This is also reflected in other pathologies and protected features, except for the coefficient of the attribute Black, which increases from 0.088 to 0.362 between the two datasets.

In summary, the obtained coefficients express and state the existence of biases in downstream predictions.

---

<sup>2</sup>Note that age is divided by 100 in our encoding, hence an increase in one year is equivalent to 0.01.



**Applying Orthogonalization** However, after applying orthogonalization, the resulting regression coefficients are estimated to be zero and exhibit p-values of one, implying that the protected feature information is successfully removed in the corrected embedding.

We visually inspect the effects of the orthogonalization in Figure 2 using the first two PCA components of the embedding before and after orthogonalization. We do this by exemplary comparing the marginal distributions of these two components for the two available sex labels (M/F) across all evaluated modalities. This visual inspection reveals that the orthogonalization procedure does not change the directions of the highest variance in the datasets and the general structure of the embedding space is preserved. However, when examining the differences in the two sex labels, an alignment in the marginal distributions can be detected. This is particularly striking for the marginals of the second principal component in the MIMIC CFM and CheSS embeddings. After applying orthogonalization, the shift between those distributions is removed, resulting in a loss of discriminative power and elimination of bias regarding this feature. In contrast, there are no or only minor visual changes in the marginals of the first two PCA components for *Pleural Effusion* (cf. Figure 2).

### 3.2 Predicting Protected Information

Apart from their influence on pathology classification, we investigate how well the protected information can be predicted directly from the embeddings themselves before and after orthogonalization. As depicted in Figure 3 and Table 4, identification of protected features in deep embeddings can be achieved with high accuracy, e.g., a patient’s sex with an AUC of 0.979 in MIMIC CFM. The orthogonalization removes the respective feature information, a classification is then not feasible anymore and results in random guessing. This does not only apply to sex and race prediction but also to the patient’s age. In the case of CheXpert’s CheSS embeddings, linear regression yields an  $R^2$  of 0.529, whereas, after correction, the  $R^2$  is  $-0.009$ . Generally, the two CLF models show the lowest AUCs when predicting sex or race.

### 3.3 Downstream Prediction Performance

Lastly, another important question is how orthogonalization influences embeddings with respect to their predictive power. Table 3 contains an overview of the estimated downstream prediction performances when training a logistic regression on both, the original and corrected embeddings, separately. The MIMIC CFM embedding has a notably higher macro-averaged AUC in comparison to CheSS and CLF (0.789 versus 0.695 and 0.679.) On CheXpert, the CLF embedding with an AUC of 0.720 yields a slightly better result than CheSS with 0.710. The orthogonalized MIMIC embeddings perform generally worse than their uncorrected counterparts containing the protected features. For CheSS and CLF, the difference in performance is  $-0.14\%$  and hence negligible, while for the CFM embeddings, the decrease is  $-1.39\%$ . However, in the case of CheXpert, the removal of the protected feature even results in a performance boost, e.g.,  $+1.83\%$  for CheSS. Removing biases hence does not automatically imply a loss in performance.

Another question concerns whether removing protected features also influences subgroup disparities. Figure 4 depicts the deviation of the subgroup AUC from the overall AUC for *Pleural Effusion* and *Cardiomegaly*. In general, the MIMIC dataset exhibits stronger disparities than CheXpert, especially in the underrepresented Asian class. Using the orthogonalization, in fact, mitigates the disparity in most cases, e.g., the *Pleural Effusion* class in MIMIC Chess from  $-12.54\%$  to  $-7.76\%$ . Inspecting the CheXpert CheSS and CLF embeddings for *Cardiomegaly*, the correction results in the full mitigation of racial bias towards Asian and Black.

## 4 Discussion

Our analysis investigates the implicit encoding of protected features age, sex, and race in three independent neural representations of MIMIC and CheXpert, and shows a significant influence of these on model predictions. Using an orthogonalization allows us to correct this effect. Our findings indicate that, post-correction, recovering protected features from the embeddings is not possible anymore and their influence on predictions is eliminated. Orthogonalization further allows to reduce subgroup disparities.

The phenomenon of bias in CXR classifiers is a highly active research area. [25] identify various sources of bias during all stages of model development and [26] account shortcut learning as a possible origin of such biases. Further, [27] detect an underdiagnosis bias in underrepresented patient populations. [10] warn about encoded protected features in latent representations of classifiers. More in-depth analyses about subgroup disparities are conducted in [13, 12]. We contribute to this discussion by not only stating the existence of biases but also by proposing additional measures to effectively remove them.

Previous work [11] already addressed potential biases in the CheXpert embeddings of CFM by testing for differences in the mean of specific subgroups in the first four PCA components. As this comes with the downside of evaluating only one protected feature isolated at a time and does not directly quantify their influence in a prediction model, we extend this idea and evaluate to what extent all protected characteristics jointly influence downstream predictions. Additionally, we discuss orthogonalization as a potential solution for the embedding bias. The authors of [28] tackle debiasing CXR classifiers by adapting the model used for prediction. Our approach, in contrast, is model-agnostic and can correct any neural representation.

The implicit usage of protected features in predictive models prompts a discussion about their role as potential biomarkers or indicators in the context of training datasets. However, if an accurate medical prediction supported by protected information is of importance, we argue that this relationship should be modeled by including the protected information as a predictor. For this purpose, orthogonalization helps to disentangle the influence of protected features and other factors and makes the influence of race, sex, age, or other information explicit instead of concealing it within the neural representations. By explicitly including metadata as separate predictors, as demonstrated in semi-structured models [15, 14], the influence of protected features can be accurately quantified and considered in the decision-making process. This approach enables a more precise and nuanced understanding of how protected features impact predictions, which can be particularly crucial for ensuring fairness and avoiding unintended biases in medical applications.

Our study has several limitations. The downstream classifier is reduced to a specific model and parameter setting, which yields a fair comparison between datasets and embeddings. We did not conduct a hyperparameter search that might enable better performance metrics; instead, our study focused on the influence of protected features concealed in a deep representation and the removal thereof. Our analysis is further based on a linear evaluation protocol that allows the application of the orthogonalization method. An extension of this method to incorporate non-linearities is non-trivial and is subject to future work. Lastly, even with the orthogonalized embedding, subgroup disparities still exist, implying more complex relationships between protected features and outcomes.

To conclude, our study confirms the results of previous research [11, 10], which addresses the existence of biases in deep feature embeddings of CXR images. We propose an orthogonalization as a way to isolate and remove the effects of protected features, providing a post-hoc measure to cleanse embeddings. Despite the removal of information in the embedding, downstream predictive power does not necessarily deteriorate and can even improve performance in some cases.

## Acknowledgments

The authors gratefully acknowledge LMU Klinikum for providing computing resources on their Clinical Open Research Engine (CORE). This work has been partially funded by the Deutsche Forschungsgemeinschaft (DFG, German Research Foundation) as part of BERD@NFDI - grant number 460037581.

## References

- [1] Alistair EW Johnson, Tom J Pollard, Nathaniel R Greenbaum, Matthew P Lungren, Chih-ying Deng, Yifan Peng, Zhiyong Lu, Roger G Mark, Seth J Berkowitz, and Steven Horng. “MIMIC-CXR-JPG, a large publicly available database of labeled chest radiographs”. In: *arXiv preprint arXiv:1901.07042* (2019).

- [2] Jeremy Irvin, Pranav Rajpurkar, Michael Ko, Yifan Yu, Silvana Ciurea-Ilcus, Chris Chute, Henrik Marklund, Behzad Haghighi, Robyn Ball, Katie Shpanskaya, et al. “Chexpert: A large chest radiograph dataset with uncertainty labels and expert comparison”. In: *Proceedings of the AAAI conference on artificial intelligence*. Vol. 33. 01. 2019, pp. 590–597.
- [3] Tobias Weber, Michael Ingrisch, Bernd Bischl, and David Rügamer. “Cascaded Latent Diffusion Models for High-Resolution Chest X-ray Synthesis”. In: *Pacific-Asia Conference on Knowledge Discovery and Data Mining*. Springer. 2023, pp. 180–191.
- [4] Pierre Chambon, Christian Bluethgen, Jean-Benoit Delbrouck, Rogier Van der Sluijs, Małgorzata Polacin, Juan Manuel Zambrano Chaves, Tanishq Mathew Abraham, Shivanshu Purohit, Curtis P Langlotz, and Akshay Chaudhari. “RoentGen: vision-language foundation model for chest x-ray generation”. In: *arXiv preprint arXiv:2211.12737* (2022).
- [5] Tobias Weber, Michael Ingrisch, Bernd Bischl, and David Rügamer. “Implicit embeddings via GAN inversion for high resolution chest radiographs”. In: *MICCAI Workshop on Medical Applications with Disentanglements*. Springer. 2022, pp. 22–32.
- [6] Guanxiong Liu, Tzu-Ming Harry Hsu, Matthew McDermott, Willie Boag, Wei-Hung Weng, Peter Szolovits, and Marzyeh Ghassemi. “Clinically accurate chest x-ray report generation”. In: *Machine Learning for Healthcare Conference*. PMLR. 2019, pp. 249–269.
- [7] Andrew B Sellergren, Christina Chen, Zaid Nabulsi, Yuanzhen Li, Aaron Maschinot, Aaron Sarna, Jenny Huang, Charles Lau, Sreenivasa Raju Kalidindi, Mozziyar Etemadi, et al. “Simplified transfer learning for chest radiography models using less data”. In: *Radiology* 305.2 (2022), pp. 454–465.
- [8] Kyungjin Cho, Ki Duk Kim, Yujin Nam, Jiheon Jeong, Jeeyoung Kim, Changyong Choi, Soyoun Lee, Jun Soo Lee, Seoyeon Woo, Gil-Sun Hong, et al. “CheSS: Chest X-Ray Pre-trained Model via Self-supervised Contrastive Learning”. In: *Journal of Digital Imaging* (2023), pp. 1–9.
- [9] Judy Wawira Gichoya, Imon Banerjee, Ananth Reddy Bhimireddy, John L Burns, Leo Anthony Celi, Li-Ching Chen, Ramon Correa, Natalie Dullerud, Marzyeh Ghassemi, Shih-Cheng Huang, et al. “AI recognition of patient race in medical imaging: a modelling study”. In: *The Lancet Digital Health* 4.6 (2022), pp. 406–414.
- [10] Ben Glocker, Charles Jones, Mélanie Bernhardt, and Stefan Winzeck. “Algorithmic encoding of protected characteristics in chest X-ray disease detection models”. In: *Ebiomedicine* 89 (2023).
- [11] Ben Glocker, Charles Jones, Mélanie Roschewitz, and Stefan Winzeck. “Risk of Bias in Chest Radiography Deep Learning Foundation Models”. In: *Radiology: Artificial Intelligence* (2023).
- [12] Monish Ahluwalia, Mohamed Abdalla, James Sanayei, Laleh Seyyed-Kalantari, Mohannad Hussain, Amna Ali, and Benjamin Fine. “The Subgroup Imperative: Chest Radiograph Classifier Generalization Gaps in Patient, Setting, and Pathology Subgroups”. In: *Radiology: Artificial Intelligence* (2023).
- [13] Laleh Seyyed-Kalantari, Guanxiong Liu, Matthew McDermott, Irene Y Chen, and Marzyeh Ghassemi. “CheXclusion: Fairness gaps in deep chest X-ray classifiers”. In: *Biocomputing 2021: proceedings of the Pacific symposium*. World Scientific. 2020, pp. 232–243.
- [14] David Rügamer. “A New PHO-rmula for Improved Performance of Semi-Structured Networks”. In: *Proceedings of the 40th International Conference on Machine Learning, ICML*. Vol. 202. Proceedings of Machine Learning Research. PMLR, 2023, pp. 29291–29305.
- [15] David Rügamer, Chris Kolb, and Nadja Klein. “Semi-structured distributional regression”. In: *The American Statistician* (2023), pp. 1–12.
- [16] Adi Ben-Israel and Thomas NE Greville. *Generalized inverses: theory and applications*. Vol. 15. Springer Science & Business Media, 2003.
- [17] Michael C Lovell. “A simple proof of the FWL theorem”. In: *The Journal of Economic Education* 39.1 (2008), pp. 88–91.

- [18] Pranav Rajpurkar, Jeremy Irvin, Kaylie Zhu, Brandon Yang, Hershel Mehta, Tony Duan, Daisy Ding, Aarti Bagul, Curtis Langlotz, Katie Shpanskaya, et al. “Chexnet: Radiologist-level pneumonia detection on chest x-rays with deep learning”. In: *arXiv preprint arXiv:1711.05225* (2017).
- [19] Mingxing Tan and Quoc V. Le. “EfficientNet: Rethinking Model Scaling for Convolutional Neural Networks”. In: *Proceedings of the 36th International Conference on Machine Learning, ICML*. Vol. 97. Proceedings of Machine Learning Research. PMLR, 2019, pp. 6105–6114.
- [20] Prannay Khosla, Piotr Teterwak, Chen Wang, Aaron Sarna, Yonglong Tian, Phillip Isola, Aaron Maschinot, Ce Liu, and Dilip Krishnan. “Supervised contrastive learning”. In: *Advances in neural information processing systems* 33 (2020), pp. 18661–18673.
- [21] Kaiming He, Xiangyu Zhang, Shaoqing Ren, and Jian Sun. “Deep residual learning for image recognition”. In: *Proceedings of the IEEE conference on computer vision and pattern recognition*. 2016, pp. 770–778.
- [22] Xinlei Chen, Haoqi Fan, Ross Girshick, and Kaiming He. “Improved baselines with momentum contrastive learning”. In: *arXiv preprint arXiv:2003.04297* (2020).
- [23] Joseph Paul Cohen, Joseph D Viviano, Paul Bertin, Paul Morrison, Parsa Torabian, Matteo Guarrera, Matthew P Lungren, Akshay Chaudhari, Rupert Brooks, Mohammad Hashir, et al. “TorchXRyVision: A library of chest X-ray datasets and models”. In: *International Conference on Medical Imaging with Deep Learning*. PMLR. 2022, pp. 231–249.
- [24] Adam Paszke, Sam Gross, Francisco Massa, Adam Lerer, James Bradbury, Gregory Chanan, Trevor Killeen, Zeming Lin, Natalia Gimelshein, Luca Antiga, et al. “Pytorch: An imperative style, high-performance deep learning library”. In: *Advances in neural information processing systems* 32 (2019).
- [25] Judy Wawira Gichoya, Kaesha Thomas, Leo Anthony Celi, Nabile Safdar, Imon Banerjee, John D Banja, Laleh Seyyed-Kalantari, Hari Trivedi, and Saptarshi Purkayastha. “AI pitfalls and what not to do: mitigating bias in AI”. In: *The British Journal of Radiology* 96.1150 (2023).
- [26] Imon Banerjee, Kamanasish Bhattacharjee, John L Burns, Hari Trivedi, Saptarshi Purkayastha, Laleh Seyyed-Kalantari, Bhavik N Patel, Rakesh Shiradkar, and Judy Gichoya. ““Shortcuts” causing bias in radiology artificial intelligence: causes, evaluation and mitigation.” In: *Journal of the American College of Radiology* (2023).
- [27] Laleh Seyyed-Kalantari, Haoran Zhang, Matthew BA McDermott, Irene Y Chen, and Marzyeh Ghassemi. “Underdiagnosis bias of artificial intelligence algorithms applied to chest radiographs in under-served patient populations”. In: *Nature medicine* 27.12 (2021), pp. 2176–2182.
- [28] Ricards Marcinkevics, Ece Ozkan, and Julia E Vogt. “Debiasing deep chest x-ray classifiers using intra-and post-processing methods”. In: *Machine Learning for Healthcare Conference*. PMLR. 2022, pp. 504–536.

MIMIC						
Training set						
	All	White	Black	Asian	Male	Female
Patients	42,148	31,936 (75.77%)	8,398 (19.93%)	1,814 (4.30%)	20,123 (47.74%)	22,025 (52.26%)
Scans	181,342	140,445 (77.45%)	33,906 (18.70%)	6,991 (3.86%)	97,361 (53.69%)	83,961 (46.21%)
Age	62.6 $\pm$ 16.6	63.9 $\pm$ 16.3	57.7 $\pm$ 16.7	62.1 $\pm$ 17.8	62.32 $\pm$ 15.8	63.0 $\pm$ 17.5
Test set						
	All	White	Black	Asian	Male	Female
Patients	257	205 (79.77%)	45 (17.51%)	7 (2.72%)	141 (54.86%)	116 (45.14%)
Scans	3,041	2,235 (73.50%)	676 (22.22%)	130 (4.27%)	1,658 (54.52%)	1,383 (45.48%)
Age	65.8 $\pm$ 12.1	66.2 $\pm$ 12.3	64.1 $\pm$ 11.9	67.4 $\pm$ 9.5	66.0 $\pm$ 11.6	65.4 $\pm$ 12.8
CheXpert						
Training set						
	All	White	Black	Asian	Male	Female
Patients	25,730	20,034 (77.86%)	1,751 (6.81%)	3,945 (15.33%)	14,165 (55.05%)	11,565 (44.95%)
Scans	76,205	59,238 (77.73%)	5,596 (7.34%)	11,371 (14.92%)	44,774 (58.75%)	31,431 (41.25%)
Age	63.1 $\pm$ 17.4	64.3 $\pm$ 17.2	55.7 $\pm$ 17.4	61.6 $\pm$ 17.4	62.5 $\pm$ 17.0	63.8 $\pm$ 17.9
Test set						
	All	White	Black	Asian	Male	Female
Patients	12,866	9,956 (77.38%)	879 (6.83%)	2,031 (15.79%)	7,091 (55.11%)	5,775 (44.89%)
Scans	38,240	29,844 (78.04%)	2746 (7.18%)	5,650 (14.278%)	22,265 (58.22%)	15,975 (41.78%)
Age	63.3 $\pm$ 17.2	64.2 $\pm$ 17.1	57.4 $\pm$ 16.3	61.1 $\pm$ 17.6	62.8 $\pm$ 16.4	63.9 $\pm$ 18.3

Table 1: Statistics of the utilized MIMIC and CheXpert subsets per split and subgroups.

	Pathology	Orthogonalized?	Age	Sex[Female]	Race[Black]	Race[Asian]
MIMIC CFM	Pleural Effusion	✗	4.246 ( $< 2e-16$ )	-0.143 ( $< 2e-16$ )	-0.694 ( $< 2e-16$ )	0.029 (0.386)
		✓	0 (1)	0 (1)	0 (1)	0 (1)
	Cardiomegaly	✗	3.490 ( $< 2e-16$ )	-0.078 ( $< 2e-16$ )	0.145 ( $< 2e-16$ )	-0.017 (0.428)
		✓	0 (1)	0 (1)	0 (1)	0 (1)
	No Finding	✗	-3.438 ( $< 2e-16$ )	0.216 ( $< 2e-16$ )	0.307 ( $< 2e-16$ )	0.157 (0.350)
		✓	0 (1)	0 (1)	0 (1)	0 (1)
MIMIC CheSS	Pleural Effusion	✗	3.529 ( $< 2e-16$ )	-0.017 (0.143)	-0.277 ( $< 2e-16$ )	0.070 (5e-4)
		✓	0 (1)	0 (1)	0 (1)	0 (1)
	Cardiomegaly	✗	2.658 ( $< 2e-16$ )	-0.007 (0.321)	0.088 ( $< 2e-16$ )	0.013 (0.386)
		✓	0 (1)	0 (1)	0 (1)	0 (1)
	No Finding	✗	-2.974 ( $< 2e-16$ )	0.250 ( $< 2e-16$ )	0.221 ( $< 2e-16$ )	-0.024 (0.150)
		✓	0 (1)	0 (1)	0 (1)	0 (1)
MIMIC CLF	Pleural Effusion	✗	3.582 ( $< 2e-16$ )	-0.193 ( $< 2e-16$ )	-0.275 ( $< 2e-16$ )	0.069 (0.001)
		✓	0 (1)	0 (1)	0 (1)	0 (1)
	Cardiomegaly	✗	2.992 ( $< 2e-16$ )	-0.099 ( $< 2e-16$ )	0.136 ( $< 2e-16$ )	-0.018 (0.255)
		✓	0 (1)	0 (1)	0 (1)	0 (1)
	No Finding	✗	-2.907 ( $< 2e-16$ )	0.217 ( $< 2e-16$ )	0.207 ( $< 2e-16$ )	-0.018 (0.279)
		✓	0 (1)	0 (1)	0 (1)	0 (1)
CheXpert CheSS	Pleural Effusion	✗	1.679 ( $< 2e-16$ )	0.135 ( $< 2e-16$ )	-0.072 (2e-5)	0.051 (1e-4)
		✓	0 (1)	0 (1)	0 (1)	0 (1)
	Cardiomegaly	✗	1.278 ( $< 2e-16$ )	0.004 (0.511)	0.362 ( $< 2e-16$ )	0.112 ( $< 2e-16$ )
		✓	0 (1)	0 (1)	0 (1)	0 (1)
	No Finding	✗	-2.347 ( $< 2e-16$ )	0.092 ( $< 2e-16$ )	-0.027 (0.120)	-0.045 (0.001)
		✓	0 (1)	0 (1)	0 (1)	0 (1)
CheXpert CLF	Pleural Effusion	✗	1.590 ( $< 2e-16$ )	0.025 (0.060)	-0.067 (5e-4)	0.036 (0.012)
		✓	0 (1)	0 (1)	0 (1)	0 (1)
	Cardiomegaly	✗	1.613 ( $< 2e-16$ )	-0.090 (2e-16)	0.454 ( $< 2e-16$ )	-0.081 (2e-9)
		✓	0 (1)	0 (1)	0 (1)	0 (1)
	No Finding	✗	-2.356 ( $< 2e-16$ )	0.039 (0.002)	-0.037 (0.057)	-0.071 ( $< 8e-7$ )
		✓	0 (1)	0 (1)	0 (1)	0 (1)

Table 2: The average coefficients (with p-values in brackets) for the impact of protected features on predictions for *Pleural Effusion*, *Cardiomegaly*, and *No Finding*. For predicting a scan’s race, the prevalent label *White* is chosen as the reference level. Cells containing p-values  $< 0.05$  are colored red marking significant influence.

Dataset:		MIMIC				CheXpert										
		CFM		CheSS		CLF		CheSS		CLF						
Embedding:																
Orthogonalized?	Enl. Cardiomed. Cardiomegaly Lung Opacity Lung Lesion Edema Consolidation Pneumonia Atelectasis Pneumothorax Pleural Effusion Pleural Other Fracture Support Devices No Finding Total	✗	✓	Δ	✗	✓	Δ	✗	✓	Δ	✗	✓	Δ			
		0.728 ± 0.009	0.721 ± 0.018	-0.97 %	0.636 ± 0.003	0.643 ± 0.007	+1.09 %	0.601 ± 0.002	0.593 ± 0.004	-1.35 %	0.621 ± 0.001	0.636 ± 0.003	+2.36 %	0.634 ± 0.000	0.639 ± 0.001	+0.78 %
		0.780 ± 0.002	0.775 ± 0.003	-0.65 %	0.750 ± 0.001	0.751 ± 0.001	+0.13 %	0.737 ± 0.000	0.736 ± 0.001	-0.14 %	0.789 ± 0.000	0.791 ± 0.001	+0.25 %	0.799 ± 0.000	0.793 ± 0.000	-0.76 %
		0.696 ± 0.003	0.684 ± 0.005	-1.75 %	0.626 ± 0.002	0.627 ± 0.004	+0.16 %	0.623 ± 0.001	0.612 ± 0.002	-1.80 %	0.685 ± 0.000	0.684 ± 0.000	-0.15 %	0.695 ± 0.000	0.690 ± 0.000	-0.72 %
		0.731 ± 0.006	0.718 ± 0.007	-1.81 %	0.623 ± 0.003	0.630 ± 0.004	+1.11 %	0.576 ± 0.009	0.591 ± 0.014	+2.54 %	0.672 ± 0.002	0.700 ± 0.002	+4.00 %	0.701 ± 0.001	0.707 ± 0.002	+0.85 %
		0.843 ± 0.001	0.837 ± 0.002	-0.72 %	0.804 ± 0.000	0.798 ± 0.000	-0.75 %	0.791 ± 0.000	0.783 ± 0.001	-1.02 %	0.791 ± 0.000	0.789 ± 0.000	-0.25 %	0.788 ± 0.000	0.783 ± 0.000	-0.64 %
		0.748 ± 0.008	0.742 ± 0.009	-0.81 %	0.648 ± 0.001	0.650 ± 0.005	+0.31 %	0.638 ± 0.003	0.640 ± 0.002	+0.31 %	0.669 ± 0.001	0.683 ± 0.001	+2.05 %	0.689 ± 0.001	0.692 ± 0.002	+0.43 %
		0.703 ± 0.005	0.704 ± 0.004	+0.14 %	0.586 ± 0.005	0.597 ± 0.009	+1.84 %	0.589 ± 0.003	0.607 ± 0.002	+2.97 %	0.610 ± 0.002	0.652 ± 0.003	+6.44 %	0.652 ± 0.001	0.659 ± 0.004	+1.06 %
		0.746 ± 0.002	0.734 ± 0.004	-1.63 %	0.702 ± 0.000	0.696 ± 0.001	-0.86 %	0.685 ± 0.001	0.671 ± 0.001	-2.09 %	0.631 ± 0.000	0.636 ± 0.001	+0.79 %	0.632 ± 0.000	0.633 ± 0.001	+0.16 %
		0.843 ± 0.005	0.830 ± 0.007	-1.57 %	0.649 ± 0.002	0.645 ± 0.005	-0.62 %	0.634 ± 0.003	0.638 ± 0.004	+0.63 %	0.732 ± 0.001	0.749 ± 0.001	+2.27 %	0.730 ± 0.001	0.740 ± 0.001	+1.35 %
		0.870 ± 0.001	0.859 ± 0.002	-1.28 %	0.802 ± 0.000	0.792 ± 0.001	-1.26 %	0.797 ± 0.000	0.781 ± 0.000	-2.05 %	0.792 ± 0.000	0.798 ± 0.000	+0.75 %	0.804 ± 0.000	0.801 ± 0.000	-0.37 %
		0.894 ± 0.009	0.874 ± 0.021	-2.29 %	0.711 ± 0.005	0.746 ± 0.011	+4.69 %	0.684 ± 0.006	0.693 ± 0.009	+1.30 %	0.723 ± 0.001	0.756 ± 0.004	+4.37 %	0.718 ± 0.001	0.718 ± 0.004	+0.00 %
0.752 ± 0.007	0.739 ± 0.013	-1.76 %	0.643 ± 0.005	0.648 ± 0.009	+0.77 %	0.642 ± 0.004	0.652 ± 0.012	+1.53 %	0.668 ± 0.001	0.682 ± 0.003	+2.05 %	0.667 ± 0.001	0.673 ± 0.003	+0.89 %		
0.909 ± 0.001	0.905 ± 0.001	-0.44 %	0.801 ± 0.000	0.801 ± 0.001	+0.00 %	0.767 ± 0.001	0.763 ± 0.001	-0.52 %	0.731 ± 0.000	0.748 ± 0.000	+2.27 %	0.711 ± 0.000	0.721 ± 0.000	+1.39 %		
0.801 ± 0.003	0.770 ± 0.005	-4.03 %	0.746 ± 0.001	0.725 ± 0.002	-2.90 %	0.747 ± 0.000	0.728 ± 0.001	-2.61 %	0.833 ± 0.000	0.824 ± 0.001	-1.09 %	0.854 ± 0.000	0.844 ± 0.000	-1.18 %		
Total		0.789 ± 0.005	0.778 ± 0.009	-1.39 %	0.695 ± 0.003	0.696 ± 0.005	-0.14 %	0.679 ± 0.003	0.678 ± 0.006	-0.14 %	0.710 ± 0.001	0.723 ± 0.002	+1.83 %	0.720 ± 0.001	0.721 ± 0.002	+0.13 %

Table 3: Prediction performance original versus orthogonalized data on the MIMIC and CheXpert datasets. The table shows the mean and standard deviation of the AUC over 10 randomly initialized runs. Additionally,  $\Delta$  depicts the percentual change from the original to the corrected embedding.

Emb.	Orthogonalized?	Age		Sex			Race [White]			Race [Black]			Race [Asian]		
		MAE	$R^2$	AUC	Sens.	Spec.	AUC	Sens.	Spec.	AUC	Sens.	Spec.	AUC	Sens.	Spec.
CFM	✗	8.040 $\pm$ 1.456	0.314 $\pm$ 0.241	0.979 $\pm$ 0.000	0.933 $\pm$ 0.025	0.902 $\pm$ 0.039	0.848 $\pm$ 0.004	0.940 $\pm$ 0.016	0.497 $\pm$ 0.049	0.871 $\pm$ 0.004	0.521 $\pm$ 0.055	0.944 $\pm$ 0.015	0.870 $\pm$ 0.005	0.179 $\pm$ 0.028	0.991 $\pm$ 0.005
	✓	10.969 $\pm$ 0.433	-0.294 $\pm$ 0.087	0.507 $\pm$ 0.031	0.775 $\pm$ 0.077	0.224 $\pm$ 0.100	0.501 $\pm$ 0.045	1.000 $\pm$ 0.000	0.000 $\pm$ 0.000	0.509 $\pm$ 0.042	0.000 $\pm$ 0.000	1.000 $\pm$ 0.000	0.464 $\pm$ 0.076	0.000 $\pm$ 0.000	1.000 $\pm$ 0.000
CheSS	✗	7.893 $\pm$ 0.066	0.331 $\pm$ 0.010	0.945 $\pm$ 0.001	0.907 $\pm$ 0.011	0.820 $\pm$ 0.016	0.761 $\pm$ 0.004	0.975 $\pm$ 0.008	0.158 $\pm$ 0.039	0.768 $\pm$ 0.003	0.143 $\pm$ 0.039	0.968 $\pm$ 0.010	0.733 $\pm$ 0.004	0.013 $\pm$ 0.008	0.997 $\pm$ 0.002
	✓	9.908 $\pm$ 0.082	-0.083 $\pm$ 0.016	0.482 $\pm$ 0.037	0.982 $\pm$ 0.024	0.013 $\pm$ 0.025	0.489 $\pm$ 0.060	1.000 $\pm$ 0.000	0.000 $\pm$ 0.000	0.478 $\pm$ 0.068	0.000 $\pm$ 0.000	1.000 $\pm$ 0.000	0.514 $\pm$ 0.048	0.000 $\pm$ 0.000	1.000 $\pm$ 0.000
CLF	✗	8.816 $\pm$ 0.063	0.161 $\pm$ 0.011	0.832 $\pm$ 0.000	0.804 $\pm$ 0.015	0.702 $\pm$ 0.016	0.631 $\pm$ 0.005	0.988 $\pm$ 0.004	0.048 $\pm$ 0.012	0.652 $\pm$ 0.005	0.050 $\pm$ 0.012	0.987 $\pm$ 0.005	0.663 $\pm$ 0.007	0.000 $\pm$ 0.000	1.000 $\pm$ 0.000
	✓	9.941 $\pm$ 0.095	-0.093 $\pm$ 0.025	0.456 $\pm$ 0.039	0.994 $\pm$ 0.007	0.007 $\pm$ 0.006	0.500 $\pm$ 0.048	1.000 $\pm$ 0.000	0.000 $\pm$ 0.000	0.498 $\pm$ 0.056	0.000 $\pm$ 0.000	1.000 $\pm$ 0.000	0.493 $\pm$ 0.084	0.000 $\pm$ 0.000	1.000 $\pm$ 0.000
CheXpert	✗	9.333 $\pm$ 0.103	0.529 $\pm$ 0.009	0.946 $\pm$ 0.000	0.912 $\pm$ 0.008	0.821 $\pm$ 0.018	0.780 $\pm$ 0.001	0.984 $\pm$ 0.007	0.136 $\pm$ 0.038	0.762 $\pm$ 0.001	0.018 $\pm$ 0.006	0.999 $\pm$ 0.001	0.816 $\pm$ 0.001	0.173 $\pm$ 0.047	0.983 $\pm$ 0.007
	✓	13.875 $\pm$ 0.035	-0.009 $\pm$ 0.005	0.499 $\pm$ 0.010	1.000 $\pm$ 0.000	0.000 $\pm$ 0.000	0.501 $\pm$ 0.007	1.000 $\pm$ 0.000	0.000 $\pm$ 0.000	0.498 $\pm$ 0.015	0.000 $\pm$ 0.000	1.000 $\pm$ 0.000	0.500 $\pm$ 0.007	0.000 $\pm$ 0.000	1.000 $\pm$ 0.000
CLF	✗	10.693 $\pm$ 0.047	0.385 $\pm$ 0.005	0.868 $\pm$ 0.000	0.854 $\pm$ 0.008	0.696 $\pm$ 0.014	0.721 $\pm$ 0.001	0.993 $\pm$ 0.003	0.040 $\pm$ 0.012	0.688 $\pm$ 0.002	0.003 $\pm$ 0.002	1.000 $\pm$ 0.000	0.764 $\pm$ 0.000	0.049 $\pm$ 0.016	0.993 $\pm$ 0.003
	✓	13.866 $\pm$ 0.035	-0.009 $\pm$ 0.005	0.496 $\pm$ 0.010	1.000 $\pm$ 0.000	0.000 $\pm$ 0.000	0.501 $\pm$ 0.008	1.000 $\pm$ 0.000	0.000 $\pm$ 0.000	0.497 $\pm$ 0.021	0.000 $\pm$ 0.000	1.000 $\pm$ 0.000	0.503 $\pm$ 0.009	0.000 $\pm$ 0.000	1.000 $\pm$ 0.000

Table 4: Regression/Classification performance for deriving protected features from an embedding vector with mean and standard deviation over 10 randomly initialized runs. The displayed metrics include mean absolute error (MAE),  $R^2$  for age regression as well as AUC, sensitivity (sens.), and specificity (spec.) for classification.



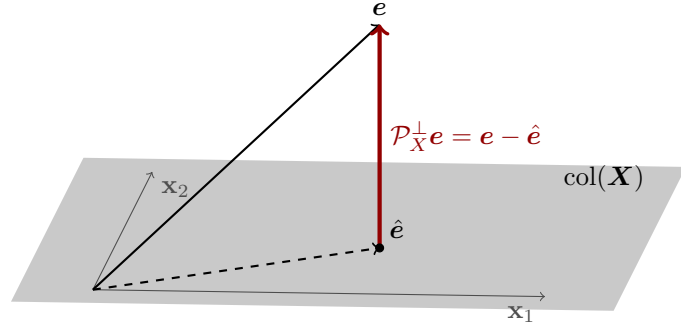


Figure 1: Geometric visualization of the orthogonalization method. The column space of the protected features ( $\text{col}(\mathbf{X})$ ) contains all the possible vectors that can be formed by taking linear combinations of the respective features, i.e. the hypothesis space of a linear model. For an embedding vector  $\mathbf{e} \in \mathbf{E}$ , the orthogonalization is equivalent to the residual between  $\mathbf{e}$  and its projection onto  $\text{col}(\mathbf{X})$ . With  $\mathcal{P}_X^\perp \mathbf{e}$  being perpendicular to  $\text{col}(\mathbf{X})$ , the influence of protected features in  $\mathbf{e}$  is neutralized.

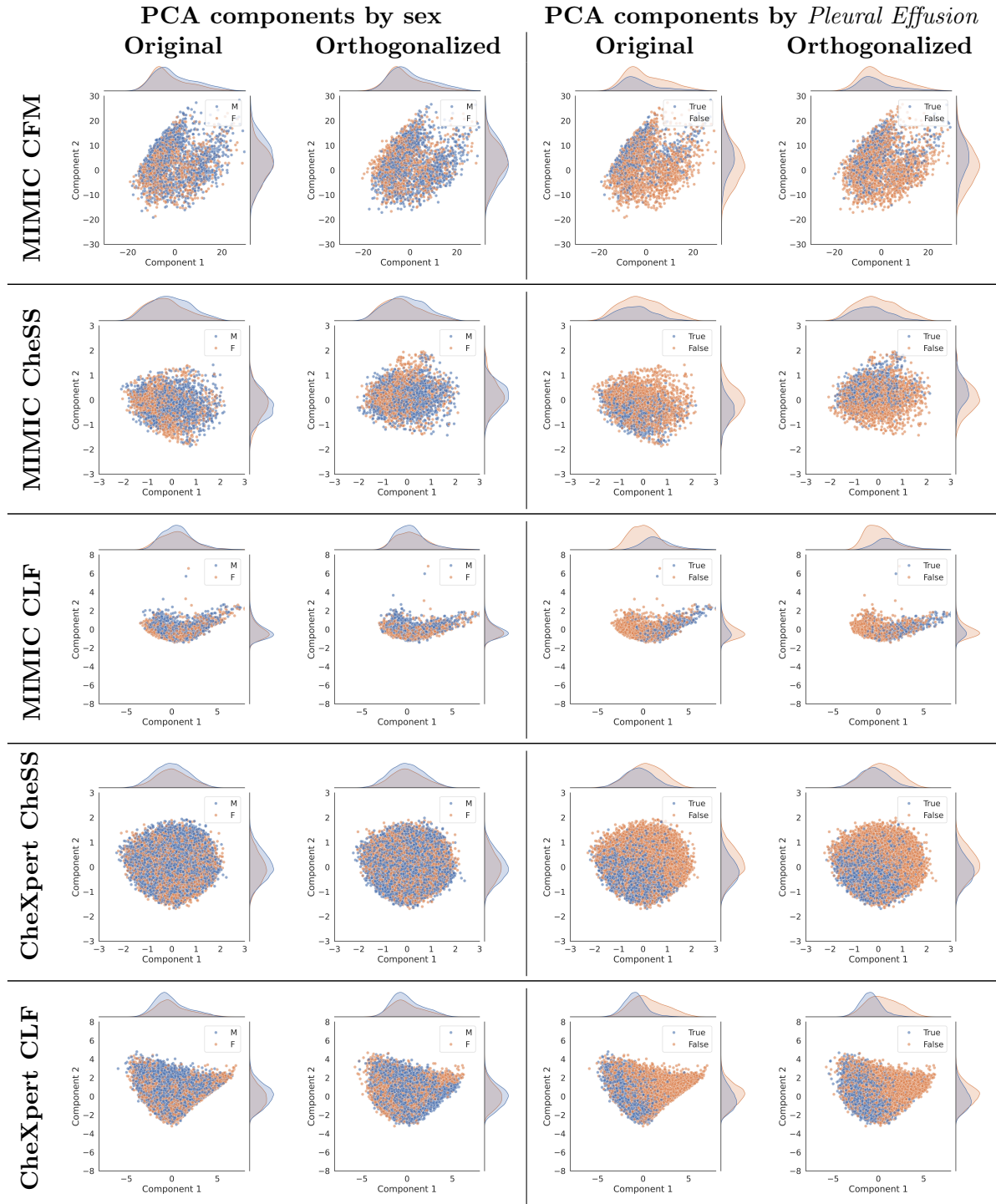


Figure 2: Marginalized distributions per sex (**left** two columns) and label *Pleural Effusion* (**right** two columns) over the PCA reduction of the original versus the orthogonalized corrected embedding.

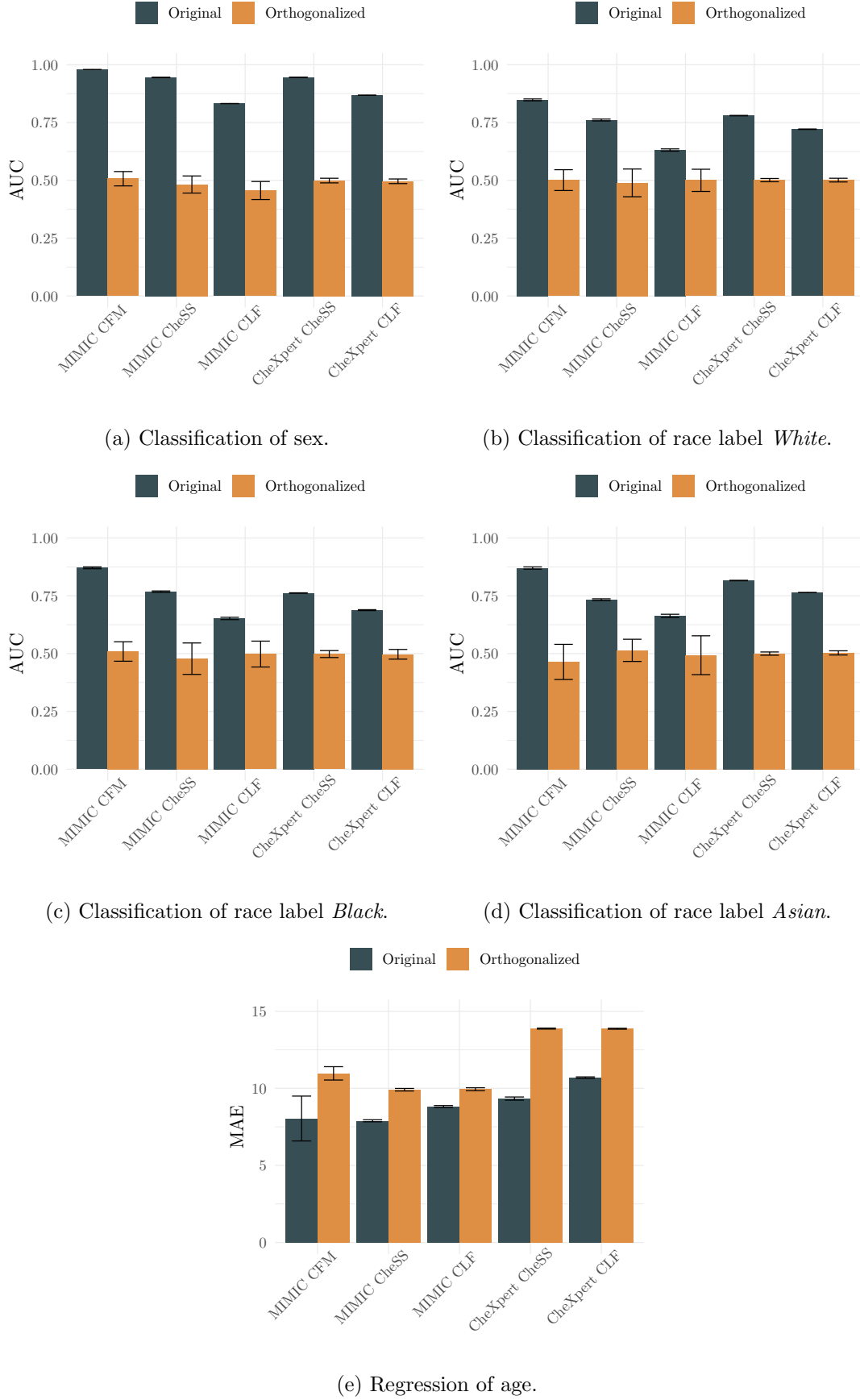
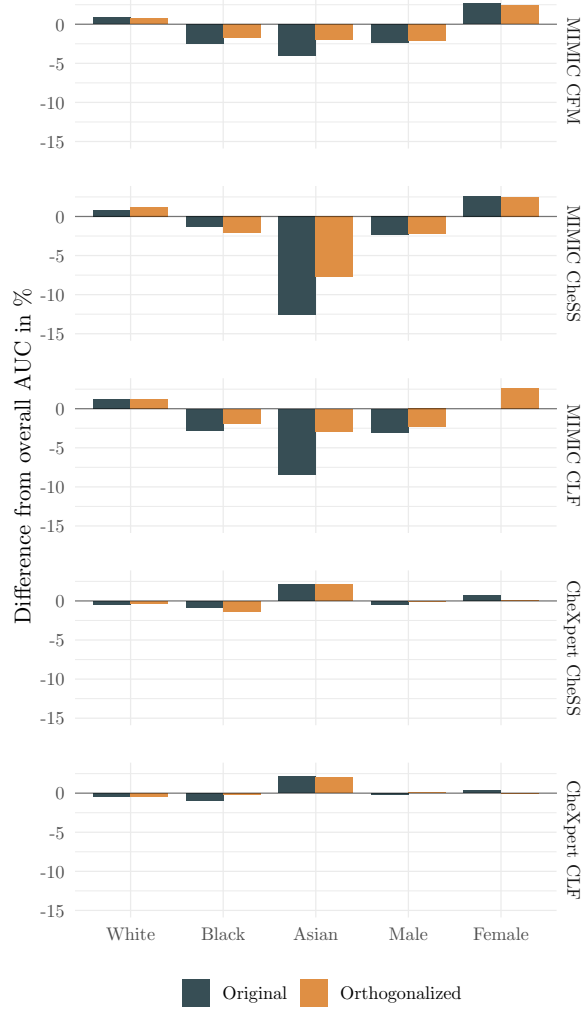
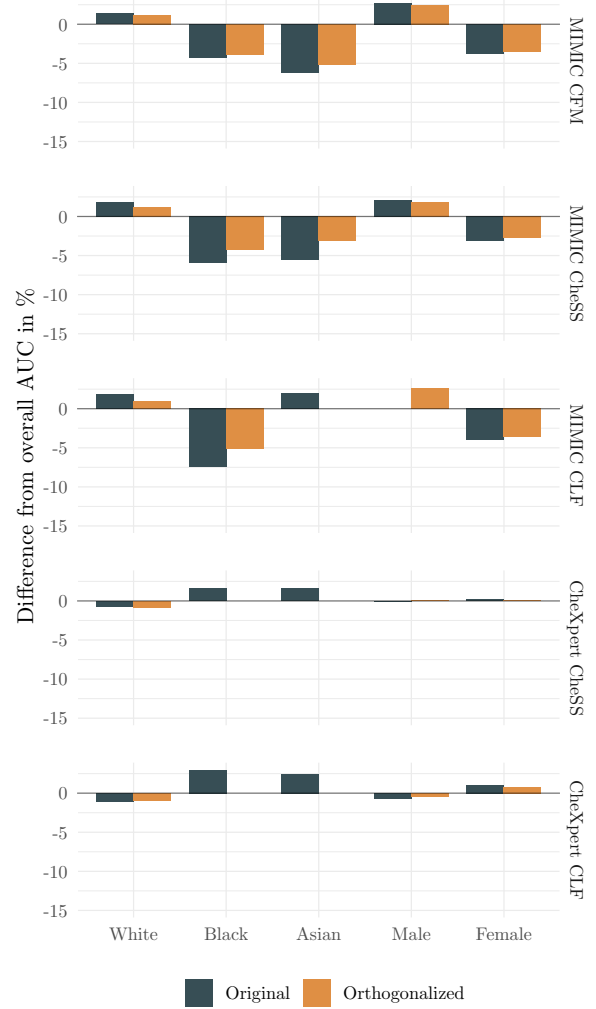


Figure 3: Regression/Classification performance for deriving protected features from an embedding vector with mean and standard deviation over 10 randomly initialized runs. The displayed metrics include mean absolute error (MAE) in years for age regression as well as AUC for classification of sex and race.



(a) Change in AUC for *Pleural Effusion*.



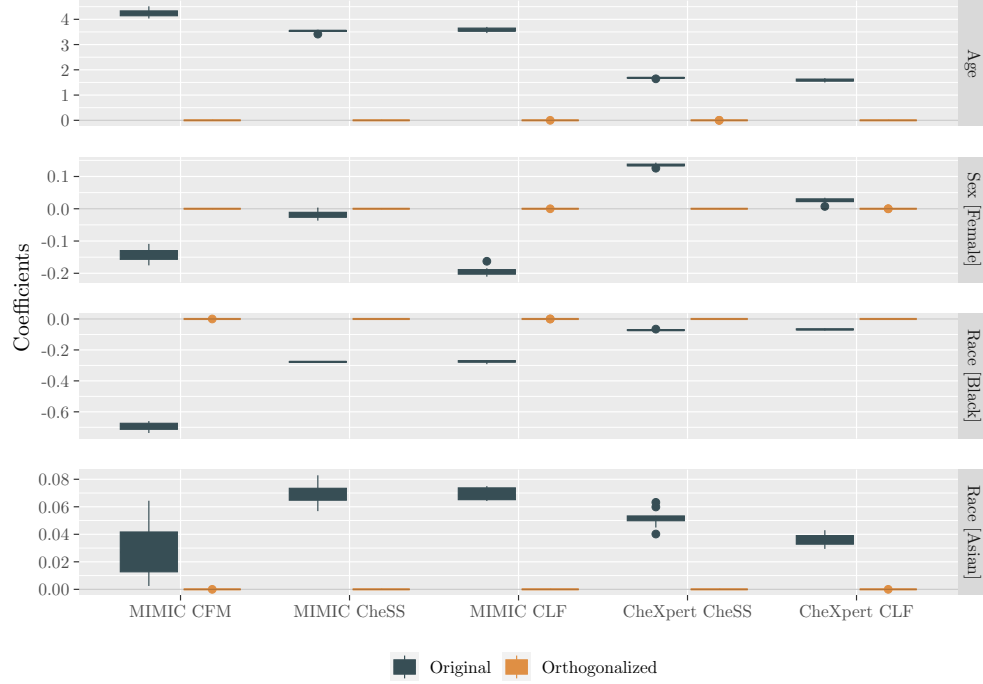
(b) Change in AUC for *Cardiomegaly*.

Figure 4: Difference from overall AUC per subgroup based on downstream classifiers for original and orthogonalized embeddings. The closer a bar is to zero, the less disparity from the mean AUC exists.

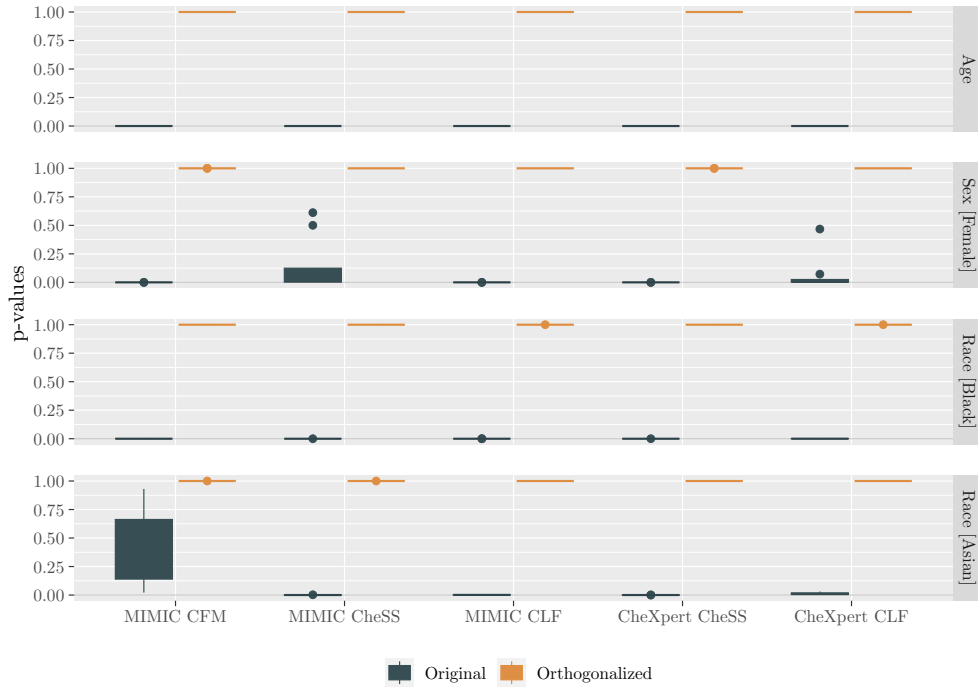
# SUPPLEMENTAL MATERIAL

## A Influence of Protected Features on Model Prediction

### A.1 Pathology: Pleural Effusion



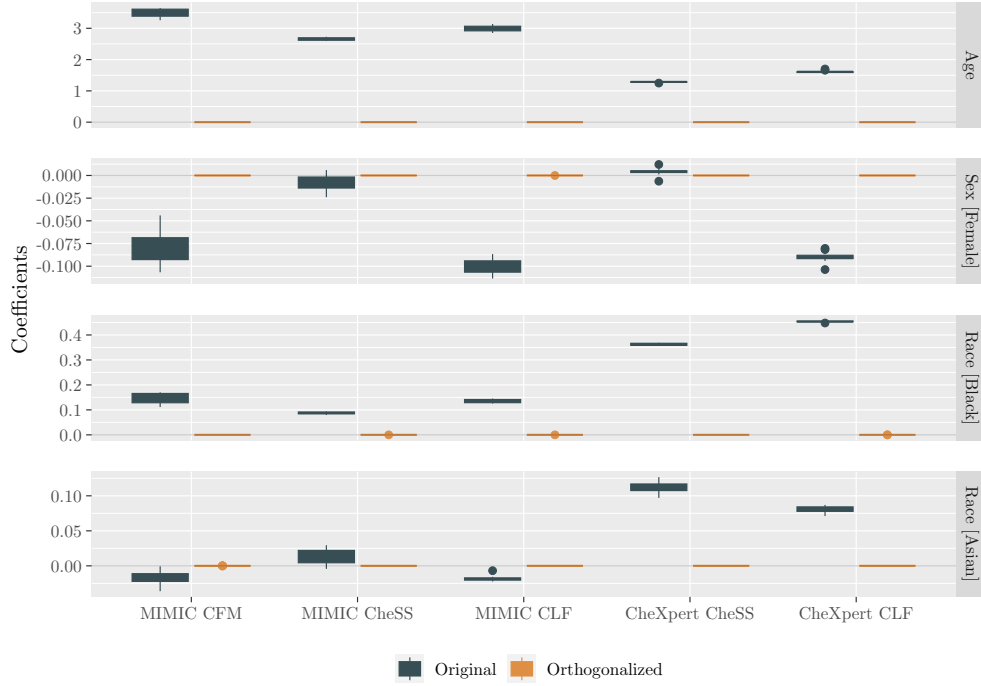
(a) Coefficients for *Pleural Effusion*.



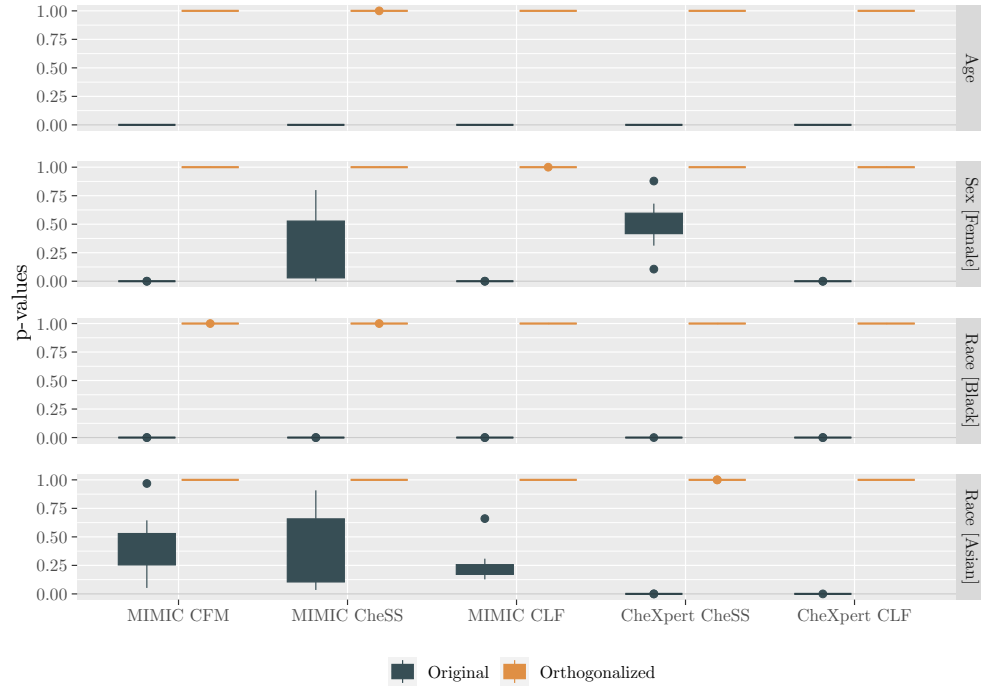
(b) p-values associated with the respective coefficients.

Figure 5: Distribution of derived coefficients and p-values for 10 downstream models per embedding and protected feature category on the label *Pleural Effusion*.

## A.2 Pathology: Cardiomegaly



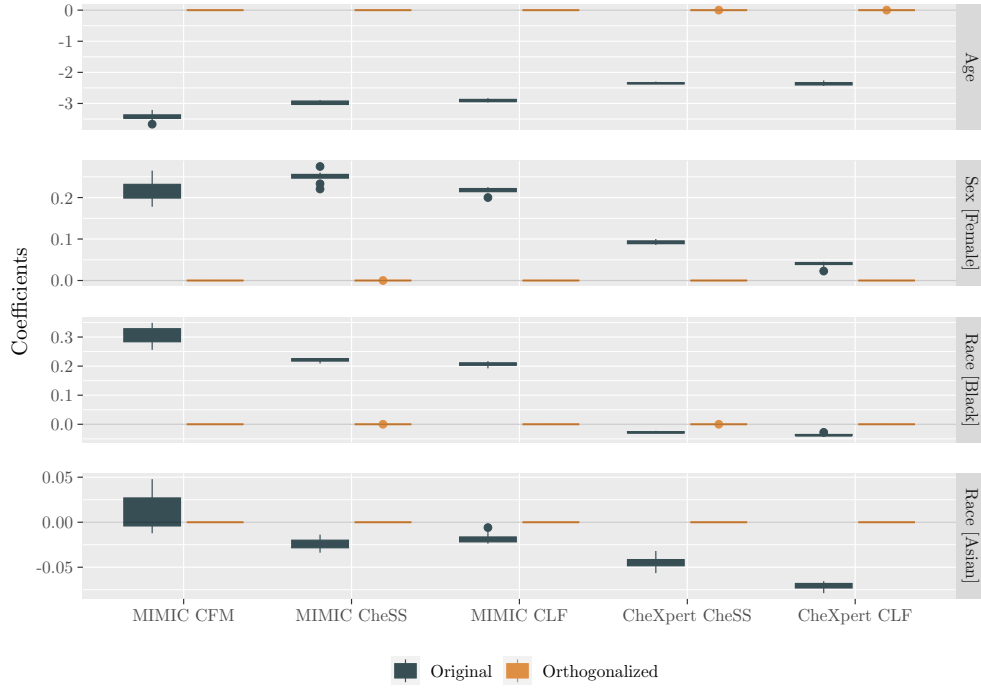
(a) Coefficients for *Cardiomegaly*.



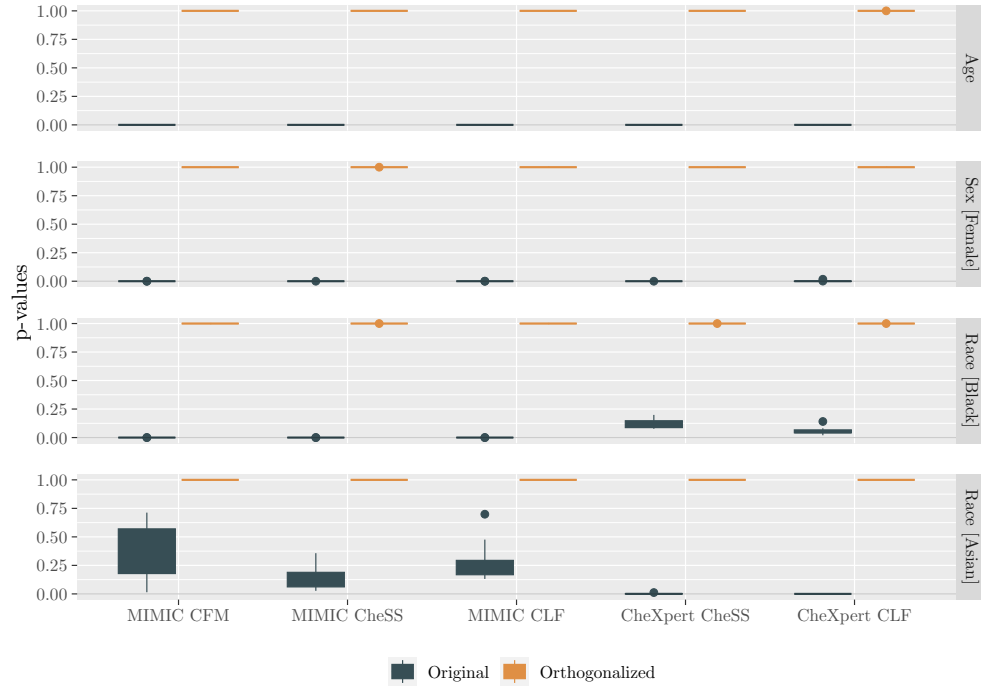
(b) p-values associated with the respective coefficients.

Figure 6: Distribution of derived coefficients and p-values for 10 downstream models per embedding and protected feature category on the label *Cardiomegaly*.

### A.3 Pathology: No Finding



(a) Coefficients for *No Finding*.



(b) p-values associated with the respective coefficients.

Figure 7: Distribution of derived coefficients and p-values for 10 downstream models per embedding and protected feature category on the label *No Finding*.